High Power Pr^{3+}:YLF CW lasers at 691.7 nm,701.4 nm, 705.0 nm and 708.7 nm

Run Fang (方 润)[1,2,3], Rongbin Dai (戴荣彬)[1,3], Huiying Xu (许惠英)[1,3], and Zhiping Cai (蔡志平)[1,3,*]

[1]Department of Electronic Engineering, Xiamen University, Xiamen 361005, China

[2]School of Physics and Electronic Science, Guizhou Normal University, Guiyang 550001, China

[3]Fujian Key Laboratory of Ultrafast Laser Technology and Applications, Xiamen University, Xiamen 361005, China

*Corresponding author: zpcai@xmu.edu.cn

Received Month X, XXXX; accepted Month X, XXXX; posted online Month X, XXXX

Lasers from $^1I_6$ to $^3F_4$ transitions were first demonstrated in a Pr^{3+}:YLF crystal by inserting a birefringent filter. Output powers up to 2.44 W, 2.10 W, 2.01 W and 2.42 W were obtained at 691.7 nm, 701.4 nm, 705.0 nm and 708.7 nm. Their slope efficiencies were 19.8%, 16.5%, 15.8% and 19.4%, respectively. The M_x^2 and M_y^2 factors were measured to be 2.29 and 2.03 at 691.7 nm, 2.23 and 1.86 at 701.4 nm, 2.31 and 2.08 at 705.0 nm, and 2.41 and 2.04 at 708.7 nm, with corresponding power fluctuations of less than 5.3%, 5.6%, 5.8%, and 2.9%.

Keywords: Pr^{3+}:YLF laser; High Power laser; Laser; Pr^{3+}:YLF crystal.
DOI: 10.3788/COLXXXXXX.XXXXXX.

1. Introduction

Deep red lights are widely used in medicine, biology, and chemistry. A photosensitizer, a benzoporphyrin derivative (BPD), was a potent generator of singlet oxygen upon activation at 692 nm [1]. BPD analogues probably owed their relative efficacy in the eradication of virus in whole blood to their activation wavelength (692 nm), which penetrated whole blood significantly more effectively than the activation wavelength (630 nm) of Photofrin. An aza-BODIPY photosensitizer (SAB) nano-particles (NPs) exhibited strong absorption around 701 nm [2]. Under 701 nm excitation, SAB NPs presented two narrow fluorescence emission peaks near 769 nm and 834 nm. The S_1 state of perylene bisimide (PBI) has an absorption band at ~705 nm corresponding to the transition of the excited electron to the higher excited state as explained later [3]. An amplified femtosecond laser, Spirit One 1040-8 was directed to a noncollinear optical parametric amplifier (NOPA), Spirit-NOPA-3H (Spectra-Physics) to generate a 705 nm femtosecond laser pulses for the PBI pump laser. However, the structure of NOPA is complex. For the photodynamic therapy (PDT) treatment, a 705 nm laser was applied to irradiate the tumor cells. Under 705 nm laser irradiation, the simultaneous PDT and photothermal therapy (PTT) destroyed tumor cells to generate DAMPs, such as pro-inflammatory cytokines and chemotactic factors, which significantly promoted dendritic cell maturation, improved the infiltration of effector T cells, and rapidly released cytokines [4]. In addition, an enhanced photoluminescence and emission intensity were shown under co-excitation with 708 nm and 532 nm lasers, which can be utilized to realize a new modality of far-field super-resolution imaging [5]. A laboratory-built Ti:sapphire chirped pulse amplification (CPA) system delivered 708 nm pulses as the pumping source, a gain bandwidth of more than one octave for a BBO crystal was obtained and 0.73–optical–cycle pulses with a pulse energy of 32 μJ at 1.8 μm was generated [6]. Similar to NOPA, the 708 nm laser with CPA has a complex structure. Visible band laser can be extended by frequency conversion [7], but the structure was also complex.

Direct generation of laser radiation has become the main part of laser Research duo to its high conversion efficiency and compact structure. Pr^{3+}:YLF crystals have been considered to be an ideal material for direct generation of visible lasers radiation because the transitions between energy levels are mainly in the visible range. In 1977, the first Pr^{3+}:YLF laser at room temperature was achieved in blue at 479 nm (corresponding to the $^3P_0 \rightarrow {}^3H_4$ transition) using a pulsed dye laser at 444 nm [8]. Since then, research on Pr^{3+}:YLF crystal lasers has continued until today. In 2014, a cyan laser of 70 mW with slope efficiency of 7% was realized at 491 nm by an optically pumped semiconductor laser (2ω-OPSL) at 480 nm [9]. In 2008, a green laser of 4.30 W with slope efficiency of 45% was reported at 522 nm by two OPSL at 479 nm [10]. In 2016, a laser of 1.70 W with slope efficiency of 49% was realized at 522 nm using a multi-mode InGaN diode laser (LD) at 444 nm [11]. In 2022, an orange laser of 3.28 W with slope efficiency of 34.2% at 604 nm was obtained by LDs [12]. In 2020, an orange laser of 4.88 W with slope efficiency of ~ 49% at 607 nm was demonstrated at an absorbed pump power of 12.15 W [13]. In 2021, a red laser of 8.14 W with slope efficiency of 51.5% at 639 nm was achieved by LDs of 24 W [14]. Furthermore, deep red lasers of 1.36 W, 3.11 W, 1.45 W, 4.50 W, and 1.90 W with slope efficiency of 15%, 31.4%, 17.8%, 41.5%, and 21.8% were reported at 696.6 nm, 698.6 nm [15], 718.5 nm, 720.8 nm [16] and 729 nm [17] by LDs, respectively. It was found that all the above lasers come from the $^3P_0$ transition, since 479 nm and 491 nm from $^3P_0 \rightarrow {}^3H_4$, 522 nm from $^3P_0 \rightarrow {}^3H_5$, 604 nm and 607 nm from $^3P_0 \rightarrow {}^3H_6$, 640 nm from $^3P_0 \rightarrow {}^3F_2$, 696 nm and 698 nm from $^3P_0 \rightarrow {}^3F_3$, 719 nm, 721 nm and 729 nm from $^3P_0 \rightarrow {}^3F_4$. However, the deep red lasers with transitions from $^1I_6$ to $^3F_4$ in Pr^{3+}:YLF crystal have not been reported so far. This may be due to the fact that the populations in $^1I_6$ is less than that in $^3P_0$, resulting in a weaker fluorescence intensity and a higher threshold. In addition, the peak emission lines from the $^1I_6$ transition are not obvious and are ignored. We are interested in the study of the lasers from the $^1I_6$ to $^3F_4$ transition, because it is helpful to expand the lasers by adding transitions between energy levels.

In this study, Pr^{3+}:YLF single-wavelength continuous-wave lasers from $^1I_6$ to $^3F_4$ transitions were reported for the first time. Maximum output powers of 2.44 W, 2.10 W, 2.01 W, 2.42 W were obtained at 691.7 nm, 701.4 nm, 705.0 nm, 708.7 nm, with slope

efficiencies of 19.8%, 16.5%, 15.8%, 19.4%, respectively. It is useful to get new laser radiation using additional transitions among energy levels.

2. Energy level transition and threshold analysis

The energy levels in Pr^{3+}:YLF were plotted as shown in Fig. 1 according to Esterowitz et al. [18]. Upon excitation at 444 nm, the $^3H_4$ ground state populations were pumped to the excited state $^3P_2$, followed by a radiation-free transition to the upper laser levels $^3P_1$, $^1I_6$, $^3P_0$, then a radiation transition to the lower laser level $^3F_4$, and finally a rapid decay to the ground state. The lasers at 691.7 nm, 701.4 nm, 705.0 nm, and 708.7 nm came from $^1I_6 \rightarrow {}^3F_4$ transitions, i.e. 21401 cm^{-1} to 6942 cm^{-1}, 21401 cm^{-1} to 7142 cm^{-1}, 21100 cm^{-1} to 6920 cm^{-1}, 21083 cm^{-1} to 6983 cm^{-1}, respectively. Under thermal equilibrium conditions, according to the Boltzmann statistics, N ($^1I_6$, 21083 cm^{-1}) / N ($^3P_0$, 20860 cm^{-1}) = 34% (at 300 K), the population distribution of the upper laser levels was mainly on the level of $^3P_0$. Therefore, the main challenge to generate lasers from $^1I_6$ transition came from the $^3P_0$ level with more populations.

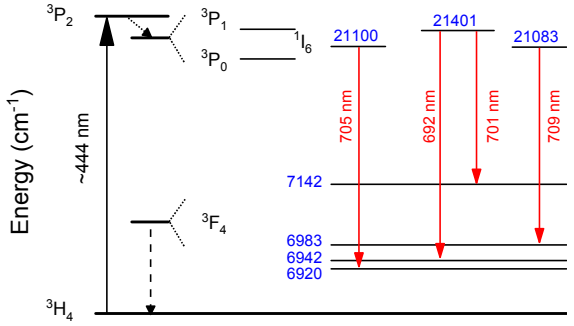

Fig. 1. The energy levels in Pr^{3+}:YLF crystals for the transitions from $^1I_6$ to $^3F_4$ at 692 nm, 701 nm, 705.0 nm and 709 nm.

Based on the fluorescence spectrum with 444 nm excitation, the emission cross sections in Pr^{3+}:YLF crystal was calculated using the F-L method [19] as shown in Fig. 2. Obviously, the emission cross-sections in the π direction is several times larger than that in the σ direction, and the lasing threshold in the π direction is much lower and easier to generate laser, so we take the π direction wavelength as the object of study. The two wavelengths (698 nm, 721 nm) with larger emission cross sections are from the transitions of $^3P_0$, while the four wavelengths (691.7 nm, 701.4 nm, 705.0 nm, 708.7 nm) with smaller emission cross sections are from the transitions of $^1I_6$. The emission cross sections at 698 nm, 721 nm are 1.07×10^{-19} cm^2, 1.78×10^{-19} cm^2. The emission cross sections at 691.7 nm, 701.4 nm, 705.0 nm, 708.7 nm are 0.15×10^{-19} cm^2, 0.15×10^{-19} cm^2, 0.13×10^{-19} cm^2, 0.15×10^{-19} cm^2, respectively. Apparently, the emission cross sections from $^3P_0$ are 7-12 times larger than those from $^1I_6$. Thus, the problem facing operation of lasers with smaller emission cross sections is the suppression of excitation at 698 nm and 721 nm. This is consistent with the results of the energy level analysis.

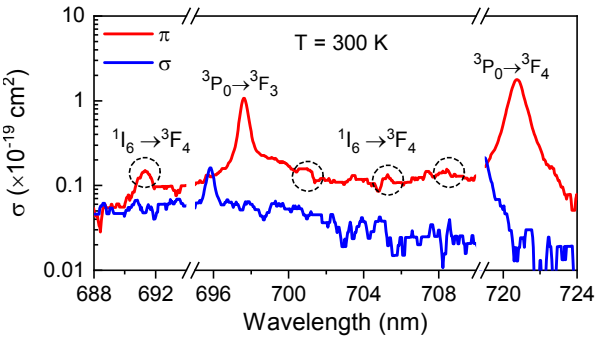

Fig. 2. Emission cross sections of Pr^{3+}:YLF crystal under 444 nm excitation. The emission cross sections from $^1I_6$ transitions at 691.7 nm, 701.4 nm, 705.0 nm and 708.7 nm are 0.15×10^{-19} cm^2, 0.15×10^{-19} cm^2, 0.13×10^{-19} cm^2 and 0.15×10^{-19} cm^2, respectively. The emission cross sections from $^3P_0$ transitions at 698 nm and 721 nm are 1.07×10^{-19} cm^2 and 1.78×10^{-19} cm^2, respectively.

3. Experimental setups

In order to realize lasers with $^1I_6 \rightarrow {}^3F_4$ transitions, an experimental setup was constructed as shown in Fig. 3. An InGaN laser diode array with a maximum output power of 24 W and a central wavelength of 444 nm (linewidth of about 2 nm) was used as the pump source. The output of the pump source is a collimated beam of approximately 5.5 × 3.8 mm^2 with vertical polarization. The quality factor of the pump beam is approximately $M_x^2 = 47$, $M_y^2 = 16$. To match the pump mode to the cavity mode, a convex lens (focal length 75 mm) is used to focus the pump beam to a waist radius of about 100 μm. To design a compact laser, a linear resonant cavity was selected for experiment. The cavity was consisting of M1 and M2 (100 mm radius of curvature). M1 was a plane mirror with high transmittance (> 98.3%) at 444 nm to improve pumping efficiency and high reflectance (> 99.8%) for light at 691.7 nm, 701.4 nm, 705.0 nm, and 708.7 nm to reduce intracavity losses. M2 was a concave mirror with high reflectivity (> 99.8%) at 691.7 nm, 701.4 nm, 705.0 nm, 708.7 nm to reduce intracavity losses. The reflectance of M1 (M2) at 698nm, 721nm was 99.99%, 99.99% (99.6%, 97.4%), respectively. We had hoped that M2 would have a high transmittance at 698 nm and 721 nm to suppress its excitation. In fact, it is almost impossible for the M2 to achieve high reflectivity at 691 nm, 701 nm and high transmittance at 698 nm at the same time. To suppress the excitation at 698 nm and 721 nm, a F-P etalon as a frequency selective device was considered but quickly ruled out because of its low rejection ratio. Fortunately, the transmittance of a birefringent filter (BF) can theoretically vary from 0 to 100% [20]. Therefore, a 2 mm thick BF with a high suppression ratio was chosen to suppress the excitation at 698 nm, 721 nm. To reduce the losses, the BF was inserted into the resonant cavity at a Brewster angle. To measure the power of the signal, a commercial blue light filter was used to filter the residual pump light.

The gain medium was a Pr^{3+}:YLF crystal that was optically polished at both ends. Pr^{3+}:YLF crystals of different lengths and concentrations were used in the experiments, such as 3 × 3 × 7 mm^3 with 0.5 at.% and 3 × 3 × 20 mm^3 with 0.15 at.%. Unfortunately, the 3 × 3 × 7 mm^3 with 0.5 at.% was damaged due to severe thermal effects. Therefore, lower concentrations (0.15 at.%) of Pr^{3+}:YLF were chosen to reduce thermal effects. To increase the absorption efficiency, a 20 mm length Pr^{3+}:YLF crystal was used. The crystal with π polarization absorption

efficiency of about 65.4% was wrapped on the side by an indium foil and placed in a water-cooled copper block to dissipate heat. The temperature of the water-cooled copper block was kept at 16 ℃ throughout the experiment.

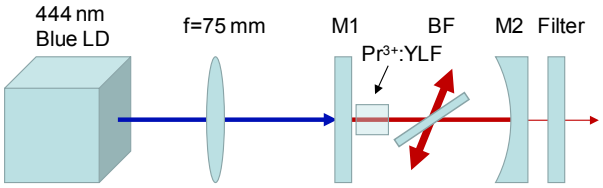

Fig. 3. Schematic diagram of the laser experiment for the transition from $^1I_6$ to $^3F_4$. LD array with 24 W output power at 444 nm. Convex lens with focal length of 75 mm. M1 with a high transmittance (> 98.3%) at 444 nm. M1and M2, with a high reflectance (> 99.8%) at 691.7 nm, 701.4 nm, 705.0 nm and 708.7 nm. BF (2 mm thick). Filter with a high reflectance in blue light region and a high transmittance at 691.7 nm, 701.4 nm, 705.0 nm, 708.7 nm.

4. Results and discussions

When the cavity length was optimized to 96 mm, the average laser spot radius was about 94 μm. Considering the negative

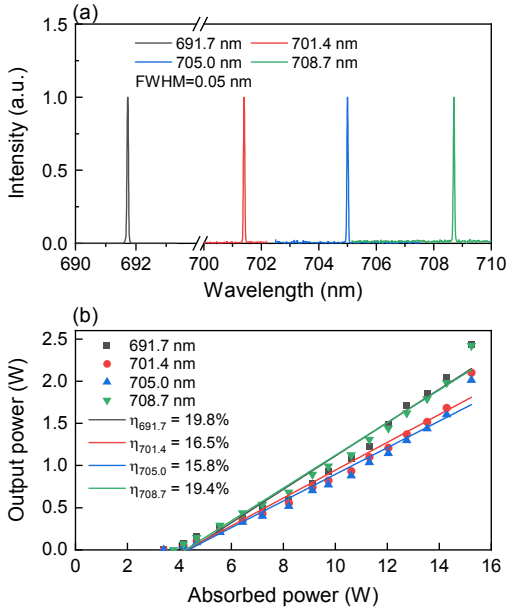

Fig. 4. (a) Normalized intensity at 691.7 nm, 701.4 nm, 705.0 nm, and 708.7 nm with 0.05 nm full width at half maximum. (b) Output powers of 2.44 W, 2.10 W, 2.01 W, 2.42 W at 691.7 nm, 701.4 nm, 705.0 nm, 708.7 nm, with slope efficiencies of 19.8%, 16.5%, 15.8%, 19.4% and corresponding threshold powers of 3.40 W, 3.40 W, 3.40 W and 3.78 W.

thermal lens of the crystal, it was possible that the laser mode matches the pump light well at this point, so that the best output was obtained as shown in Fig. 4. The full width at half maximum (FWHM) of spectrum was measured to be 0.05 nm at 691.7 nm, 701.4 nm, 705.0 nm and 708.7 nm using an Advantest Q8384 optical spectrum analyzer (resolution of 0.05 nm), as shown in Fig. 4(a). Since the spectral linewidth is equal to the resolution of the optical spectrum analyzer, the actual linewidth may be less than 0.05 nm. Such a narrow spectrum may be attributed to the use of BF, competition among modes in the cavity, and the laser operating at several times the threshold power. At the same time, the maximum output power of the laser was obtained when the absorbed power of the crystal was about 15.6 W (corresponding to a pump power of 24 W). Using an optoelectronic power meter (THORLABS S425C-L), output powers of 2.44 W, 2.10 W, 2.01 W and 2.42 W were demonstrated at 691.7 nm, 701.4 nm, 705.0 nm and 708.7 nm as shown in Fig. 4(b), with slope efficiencies of 19.8%, 16.5%, 15.8% and 19.4%, respectively. The corresponding threshold powers were 3.40 W, 3.40 W, 3.40 W and 3.78 W, respectively. In addition, both M1 and M2 have high reflectivity for the laser, so the reflected output on both sides of BF is the output of the laser.

To assess the stability of the power, the output power was recorded over 150 minutes (10-minute interval) as shown in Fig. 5. Minimum powers of 2.41 W, 2.08 W, 1.99 W, 2.39 W, maximum powers of 2.54 W, 2.20 W, 2.11 W, 2.46 W and average powers of 2.47 W, 2.14 W, 2.05 W, 2.42 W were obtained at 691.7 nm, 701.4 nm, 705.0 nm and 708.7 nm, respectively. From Fig. 5, standard deviations of 0.045 W, 0.046 W, 0.041 W and 0.021 W and peak-to-peak power fluctuations of 2.47 ± 0.06 W (5.3%), 2.14 ± 0.06 W (5.6%), 2.05 ± 0.06 W (5.8%) and 2.42 ± 0.03 W (2.9%) were calculated.

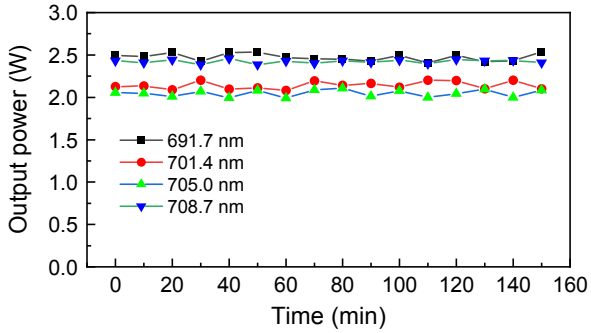

Fig. 5. Peak-to-peak power fluctuations of 2.47 ± 0.06 W, 2.14 ± 0.06 W, 2.05 ± 0.06 W and 2.42 ± 0.03 W at 691.7 nm, 701.4 nm, 705.0 nm and 708.7 nm, respectively.

To evaluate the beam quality, the beam diameters in the horizontal and vertical directions were measured at different positions on both sides of the beam waist by CCD. The beam

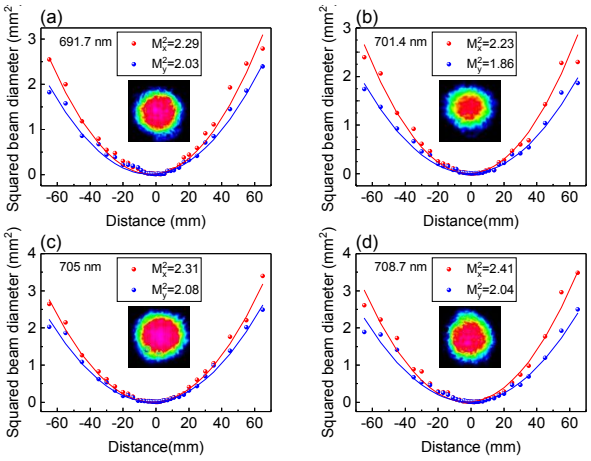

Fig. 6. (a) Beam quality M_x^2, M_y^2 factors of 2.29, 2.03 at 691.7 nm. (b) M_x^2, M_y^2 factors of 2.23, 1.86 at 701.4 nm. (c) M_x^2, M_y^2 factors of 2.31, 2.08 at 705.0 nm. (d) M_x^2, M_y^2 factors of 2.41, 2.04 at 708.7 nm.

quality factors M^2 of the laser were calculated using ISO-11164. As shown in Fig. 6, beam quality M_x^2 and M_y^2 factors were estimated to be 2.29 and 2.03 at 691.7 nm, 2.23 and 1.86 at 701.4 nm, 2.31 and 2.08 at 705.0 nm, and 2.41 and 2.04 at 708.7 nm. It can be inferred from the M^2 factors that the output may include some higher order modes. The laser spots captured by the CCD were embedded in Fig. 6(a), (b), (c) and (d), from which it can be seen that the output beams are approximately circular Gaussian light.

5. Conclusion

The continuous wave lasers with transition from $^1I_6$ to $^3F_4$ were demonstrated in the Pr^{3+}:YLF crystal for the first time. The lasers at 691.7 nm, 701.4 nm, 705.0 nm and 708.7 nm were successfully achieved, with output powers of 2.44 W, 2.10 W, 2.01 W, 2.42 W and slope efficiencies of 19.8%, 16.5%, 15.8%, 19.4%, respectively. Besides the careful tuning in the experiments, the following points are worth mentioning. Faced with the problem of small emission cross section and high threshold at new wavelengths, a high-power pump source (24 W LD array) was used, which inevitably brought about serious thermal effects. Experiments showed the use of crystals with low doping concentration to improve the damage resistance threshold of the crystal, which is the first point worth noting. The second point is the design of a closed cavity with a simple structure consisting of two mirrors to reduce losses. The third point is the use of BF with high suppression ratio in the case where the coating is difficult to suppress the 698 nm, 721 nm excitations. In conclusion the method of carefully designing additional energy level transition to excite generation of laser radiation with new wavelengths has been successful. We expect that this method will be widely used to develop lasers with a possibility to generate radiation with new wavelengths.

Funding

This work is supported by the National Natural Science Foundation of China (NSFC) (Grant No. 61975168) and National Key Research and Development Program (2020YFC2200400).

References

1. H. C. Neyndorff, D. L. Bartel, F. Tufaro, and J. G. Levy, "Development of a model to demonstrate photosensitizer-mediated viral inactivation in blood", Transfusion 30, 485 (1990).
2. Q. Y. Tang, Z. J. Cheng, N. Yang, Q. Z. Lia, P. Wang, D. P. Chen, W. J. Wang, X. J. Song, and X. C. Dong, "Hydrangea-structured tumor microenvironment responsive degradable nanoplatform for hypoxic tumor multimodal imaging and therapy", Biomaterials 205, 1 (2019).
3. D. Yoshioka, D. Fukuda, and Y. Kobayashi, "Green and far-red-light induced electron injection from perylene bisimide to wide bandgap semiconductor nanocrystals with stepwise two-photon absorption process", Nanoscale 13, 1823 (2021).
4. Y. Sun, Y. F. Zhang, Y. Gao, P. Wang, G. He, N. T. Blum, J. Lin, Q. H. Liu, X. B. Wang, and P. Huang, "Six Birds with One Stone: Versatile Nanoporphyrin for Single-Laser-Triggered Synergistic Phototheranostics and Robust Immune Activation", Adv. Mater. 32, 2004481 (2020).
5. M. Kianinia, C. Bradac, B. Sontheimer, F. Wang, T. T. Tran, M. Nguyen, S. Kim, Z. Q. Xu, D. Jin, A. W. Schell, C. J. Lobo, I. Aharonovich, and M. Toth, "All-optical control and super-resolution imaging of quantum emitters in layered materials", Nat. Commun. 9, 874 (2018).
6. Y. C. Lin, Y. Nabekawa, and K. Midorikawa, "Optical parametric amplification of sub-cycle shortwave infrared pulses", Nat. Commun. 11, 3413 (2020).
7. Y. M. Duan, H. Y. Zhu, G. Zhang, and D. Y. Tang, "Multiple visible wavelength switchable cascaded self-Raman laser based on selective wave-mixing mechanism", Appl. Phys. Lett. 123, 261102 (2023).
8. L. Esterowitz, R. Allen, M. Kruer, F. Bartoli, L. S. Goldberg,H. P. Jenssen, A. Linz, and V.O. Nicolai, "Blue light emission by a Pr:$LiYF_4$–laser operated at room Temperature", J. Appl. Phys. 48, 650 (1977).
9. P. W. Metz, K. Hasse, D. Parisi, N.-O. Hansen, C. Kränkel, M. Tonelli, and G. Huber, "Continuous-wave Pr^{3+}:BaY_2F_8 and Pr^{3+}:$LiYF_4$ lasers in the cyan-blue spectral region", Opt. Lett. 39, 5158 (2014).
10. V. Ostroumov, and W. Seelert, "1 W of 261 nm cw generation in a Pr^{3+}:$LiYF_4$ laser pumped by an optically pumped semiconductor laser at 479 nm", Proc. of SPIE. 6871, 68711K (2008).
11. S. Y. Luo, X. G. Yan, Q. Cui, B. Xu, H. Y. Xu, and Z. P. Cai, "Power scaling of blue-diode-pumped Pr:YLF lasers at 523.0, 604.1, 606.9, 639.4, 697.8 and 720.9 nm", Opt. Commun. 380, 357 (2016).
12. X. J. Lin, S. H. Ji, Q. C. Feng, X. R. Liu, R. Fang, B. Xiao, W. S. Li, H. Y. Xu, and Z. P. Cai, "Heat-induced wavelength-switchable high-power CW orange Pr^{3+}:YLF lasers", J. Lumin. 243, 118627 (2022).
13. X. J. Lin, Y. Zhu, S. H. Ji, W. S. Li, H. Y. Xu, and Z. P. Cai, "Highly efficient LD-pumped 607 nm high-power CW Pr^{3+}:YLF lasers", Opt. Laser Technol. 129, 106281 (2020).
14. X. J. Lin, M. P. Chen, Q. C. Feng, S. H. Ji, S. W. Cui, Y. Zhu, B. Xiao, W. S. Li, H. Y. Xu, and Z. P. Cai, "LD-pumped high-power CW Pr^{3+}:YLF Laguerre-Gaussian lasers at 639 nm", Opt. Laser Technol. 142, 107273 (2021).
15. W. H. Cao, Z. D. Dai, R. Fang, Z. Y. Wang, Y. C. Xue, B. Xiao, H. Y. Xu, and Z. P. Cai, "Watt-level laser operation of Pr^{3+}:YLF at 696 and 698 nm", Chin. Opt. Lett. 21, 041404 (2023).
16. X. R. Liu, Z. Li, C. K. Shi, B. Xiao, R. Fang, Y. C. Xue, Q. C. Feng, X. J. Lin, Y. Zhu, G. Z. Xu, H. Y. Xu, and Z. P. Cai, "LD-pumped high-power continuous-wave Pr^{3+}:YLF deep red lasers at 718.5 and 720.8 nm", Laser Phys. 32, 025801 (2022).

17. R. Fang, Z. P. Cai, and H.Y. Xu, "Watt-level 729-nm Pr^{3+}:YLF laser pumped by an InGaN laser diode", Opt. Lett. 47, 4267 (2022).
18. L. Esterowitz, F. J. Bartoli, R. E. Allen, D. E. Wortman, C. A. Morrison, and R. P. Leavitt, "Energy levels and line intensities of Pr^{3+} in $LiYF_4$", Phys. Rev. B 19, 6442 (1979).
19. H. P. Weber, P. Liao, and B. C. Tofield, "Emission Cross Section and Fluorescence Efficiency of Nd-Pentaphosphate", IEEE J. Quantum. Elec. 10, 563 (1974).
20. X. Lin, Q. C. Feng, X. R. Liu, S. H. Ji, B. Xiao, H. Y. Xu, and Z. P. Cai, "Wavelength extension and power improvement of red Pr^{3+}:YLF lasers", Opt. Lett. 47, 3051 (2022).